SCIENTIFIC REPORTS

OPEN

Flexibly tunable high-quality-factor induced transparency in plasmonic systems

Received: 10 October 2017
Accepted: 4 January 2018
Published online: 24 January 2018

Hua Lu[1], Xuetao Gan[1], Dong Mao[1], Baohua Jia[2] & Jianlin Zhao[1]

The quality (Q) factor and tunability of electromagnetically induced transparency (EIT)-like effect in plasmonic systems are restrained by the intrinsic loss and weak adjustability of metals, limiting the performance of the devices including optical sensor and storage. Exploring new schemes to realize the high Q-factor and tunable EIT-like effect is particularly significant in plasmonic systems. Here, we present an ultrahigh Q-factor and flexibly tunable EIT-like response in a novel plasmonic system. The results illustrate that the induced transparency distinctly appears when surface plasmon polaritons excited on the metal satisfy the wavevector matching condition with the guided mode in the high-refractive index (HRI) layer. The Q factor of the EIT-like spectrum can exceed 2000, which is remarkable compared to that of other plasmonic systems such as plasmonic metamaterials and waveguides. The position and lineshape of EIT-like spectrum are strongly dependent on the geometrical parameters. An EIT pair is generated in the splitting absorption spectra, which can be easily controlled by adjusting the incident angle of light. Especially, we achieve the dynamical tunability of EIT-like spectrum by changing the Fermi level of graphene inserted in the system. Our results will open a new avenue toward the plasmonic sensing, spectral shaping and switching.

Electromagnetically induced transparency (EIT) is a quantum destructive interference effect that occurs in atomic systems, inducing a narrow transparency window in the original absorption spectrum[1]. In the transparency window, the dispersion features of the atomic medium can be drastically modified, which has promising applications in nonlinear optics, optical data storage and ultrafast optical switching[2]. Until now, the EIT effect has been demonstrated in various media. Behroozi *et al.* reported the generation of an EIT in the ultracold gas of sodium atoms, and reduced the light speed to 17 m/s by means of the EIT effect[3]. Qi and Lazoudis *et al.* realized the EIT effect in the Doppler-broadened lithium gas[4] and acetylene photonic mirocell[5]. The EIT phenomenon was also observed by Lazoudis *et al.* in the sodium molecules generated within the heat-pipe oven[6]. In the classical systems, recently, a new kind of optical phenomena was observed and regarded as the EIT-like effect due to its remarkable analog of the EIT effect in atomic systems[7–10]. This kind of EIT-like effect attracts wide attentions because of its dispersion properties similar to those of EIT in atomic systems[7–10]. Especially, the EIT-like effect could find significant applications in chip-scale optical signal processing[8]. Naweed *et al.* observed the EIT-like response in coupled fused-silica microspheres and found the mode interference mechanism of EIT-like effect[7]. Xu *et al.* experimentally demonstrated the formation of EIT-like spectrum in all-optical silicon resonator systems[8]. Xiao *et al.* theoretically proposed the all-optical generation of multiple EIT in the drop-filter waveguide systems[9]. The performance (e.g., footprint and light confinement) of the traditional optical systems are inevitably restrained by the diffraction limit of light. Surface plasmon polaritons (SPPs) enable to confine light at sub-wavelength scale and overcome the diffraction limit of light, providing an excellent platform for nanoscale plasmonic control and elements[11–28]. Fortunately, the analog of the EIT effect was successfully observed in plasmonic systems such as plasmonic metamaterials[11–17] and waveguides[18–21,28]. The EIT-like response in plasmonic systems could find the particular applications in ultrasmall photonic devices, for example the slow-light elements[20], nanoscopic coherent light source[21], nanosensors[27] and nanofilters[28]. The high quality (Q) factor and dynamic tunability of plasmonic EIT-like response are of importance for improving the device performance and broadening the applications of

[1]MOE Key Laboratory of Material Physics and Chemistry under Extraordinary Conditions, and Shaanxi Key Laboratory of Optical Information Technology, School of Science, Northwestern Polytechnical University, Xi'an, 710072, China. [2]Centre for Micro-Photonics, Faculty of Science, Engineering and Technology, Swinburne University of Technology, Hawthorn, Victoria, 3122, Australia. Correspondence and requests for materials should be addressed to H.L. (email: hualu@nwpu.edu.cn) or J.Z. (email: jlzhao@nwpu.edu.cn)

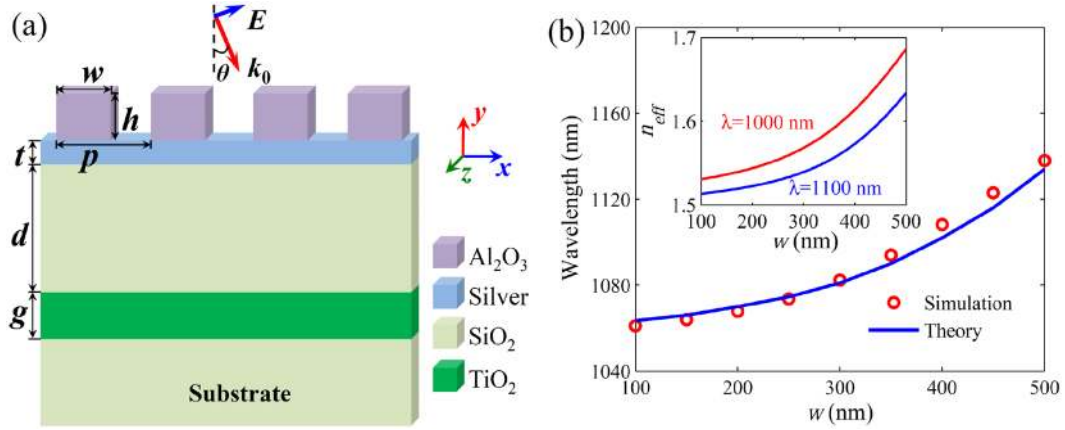

Figure 1. Schematic and excited SPP wavelengths. (**a**) Schematic of the plasmonic system composed of a Al_2O_3 ($n_a = 1.76$) grating and a silver film coated on dielectric layers. p, w and h are the pitch, width and height of Al_2O_3 grating, respectively. t, g and d are the thicknesses of silver, HRI (TiO_2, $n_t = 2.13$) and spacer (SiO_2, $n_s = 1.45$) layers, respectively. θ is the incident angle of light. (**b**) Wavelengths of excited SPP modes as a function of w. The inset shows the effective refractive indices (ERI) of SPP modes with different w.

EIT-like effect[27–31]. However, the Q factor and tunability of plasmonic EIT-like effect are generally hindered by the intrinsic loss and weak controllability of metal-based plasmonics in visible and near-infrared regions[11,20]. Exploring new ways to realize flexibly tunable high-Q-factor EIT-like effect in plasmonic systems is particularly meaningful and challenging.

Here, we propose a novel plasmonic system composed of a dielectric grating and a metallic film coated on the dielectric layers, and investigate its absorption spectral characteristics. The results illustrate that a classical analog of EIT effect can be observed in the absorption spectrum due to the satisfaction of wavevector matching condition between the SPP mode on the metallic film and guided mode in the high-refractive index (HRI) layer. The excited SPP mode destructively interferes with the coupled guided mode, resulting in the vanishment of SPP field and the appearance of transparency window in the absorption spectrum. Especially, we find that the EIT-like spectrum possesses an ultrahigh Q factor of >2000 and can be significantly tailored by adjusting the grating width, spacer thickness, HRI layer thickness and refractive index of HRI layer. By tuning the incident angle of light, a controllable EIT pair can be generated in the splitting absorption spectrum. Moreover, the flexible tunability of EIT-like spectrum is achieved by adjusting the Fermi level of graphene inserted in the HRI layer. The results may provide a new pathway toward the high-efficiency plasmonic sensing, spectral shaping and switching.

Results

Model and analytical theory for SPPs. As shown in Fig. 1(a), the plasmonic system consists of a Al_2O_3 grating and a metallic (silver) film coated on the $SiO_2/TiO_2/SiO_2$ layers. In this system, p, w and h stand for the pitch, width and height of the Al_2O_3 grating, respectively. t and g represent the thicknesses of metal and TiO_2 layers, respectively. d is the thickness of SiO_2 spacer between the metal and TiO_2 layers. Firstly, the light is assumed to be normally incident ($\theta = 0$). The dielectric grating is used to compensate the wavevector mismatch between the incident light and SPPs for the excitation of transverse magnetic (TM) SPP mode on the metallic film. It should be noted that the function of this grating is different from that of surface grating structure in diode lasers[32]. For the multilayer with a metallic film, the dispersion relation of the SPP mode can be derived from the Maxwell's equations and the boundary conditions. The SPP dispersion relation can be described as

$$e^{-2k_a h} = \frac{(1+\varepsilon_a k_0)}{(1+\varepsilon_c k_a)}\frac{(1+\psi)(1+\varphi)+(1-\psi)(1-\varphi)e^{-2k_m t}}{(1-\psi)(1+\varphi)+(1+\psi)(1-\varphi)e^{-2k_m t}}. \quad (1)$$

In Eq. (1), $\psi = \varepsilon_a k_m/\varepsilon_m k_a$ and $\varphi = \varepsilon_m k_s/\varepsilon_s k_m$. Here, $k_a = (\beta^2_{SPP} - \varepsilon_a k_0^2)^{1/2}$, $k_m = (\beta^2_{SPP} - \varepsilon_m k_0^2)^{1/2}$ and $k_s = (\beta^2_{SPP} - \varepsilon_s k_0^2)^{1/2}$ are the wavevectors of light in the Al_2O_3 grating, metal and SiO_2 layers, respectively. $\beta_{SPP} = k_0 n_{eff}$ is the SPP propagation constant and n_{eff} is the effective refractive index (ERI) of SPP mode. $k_0 = 2\pi/\lambda$ is the wavevector of incident light, and λ is the incident wavelength. $\varepsilon_a = \varepsilon_c(1-f) + \varepsilon_A f$ is equivalent to the relative permittivity of grating layer, and $f = w/p$ is the duty cycle of grating[33]. ε_m, ε_s ($=n_s^2$), ε_A ($=n_a^2$) and ε_c ($=1$) are the relative permittivities of the metal, SiO_2, Al_2O_3 and air, respectively. The relative permittivity of the metal can be described by the Drude model: $\varepsilon_m = \varepsilon_\infty - \omega_p^2/[\omega(i\gamma+\omega)]$[34], where $\omega = 2\pi c/\lambda$ is the angular frequency of light, and c is the speed of light in vacuum. ε_∞, γ and ω_p stand for the relative permittivity at the infinite frequency, electron collision frequency and bulk plasma frequency, respectively. For silver, these parameters can be set as $\varepsilon_\infty = 3.7$, $\gamma = 0.018$ eV and $\omega_p = 9.1$ eV[35]. The SPP mode on the metallic film can be effectively excited once the following phase-matching condition is satisfied,

$$\mathrm{Re}(\beta_{SPP}) - k_0 \sin\theta = \pm m\frac{2\pi}{p}, \quad (2)$$

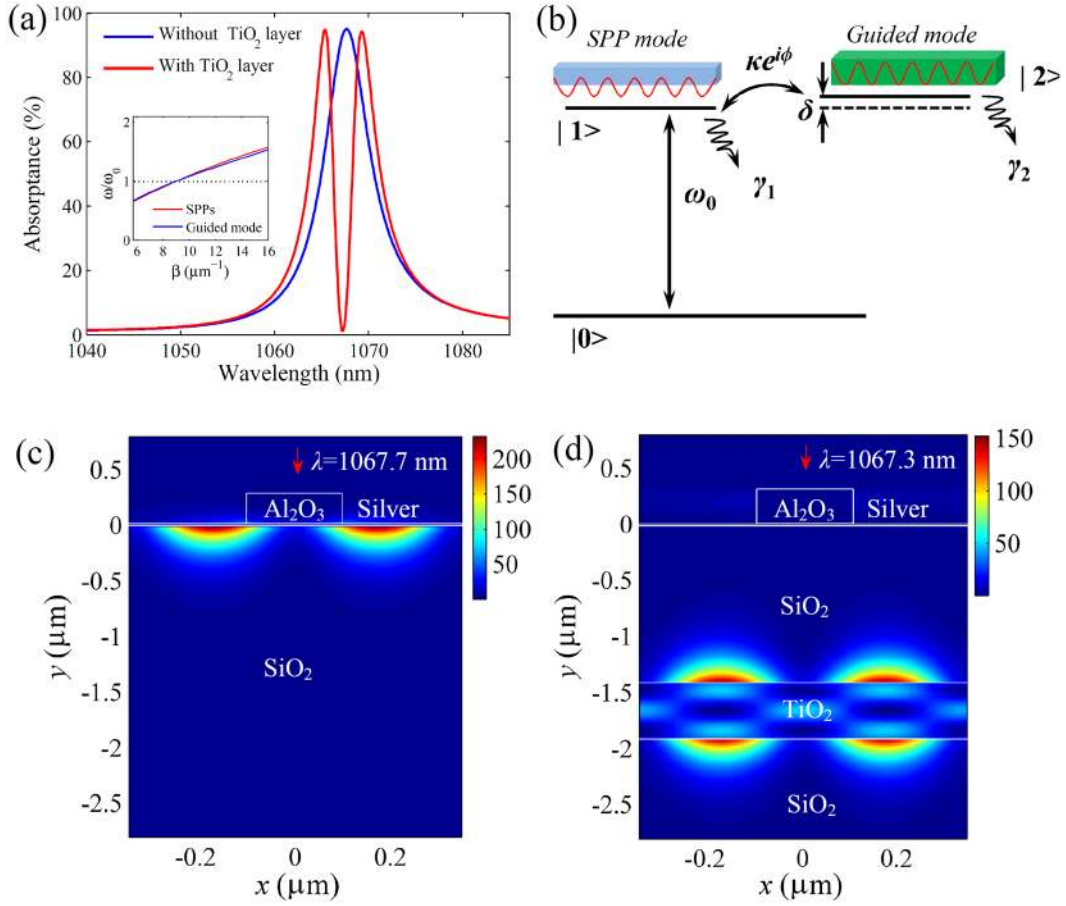

Figure 2. Spectral response, theoretical model and field distributions of EIT-like effect. (**a**) Absorption spectra of the structure without and with the TiO_2 layer. The inset shows the dispersion relations of the SPP mode on the silver film and the guided mode in the TiO_2 layer. (**b**) Coupled three-level model of the EIT-like effect in our system. (**c**) Field distribution $|E|^2$ at the absorption wavelength ($\lambda = 1067.7$ nm) in the structure without the TiO_2 layer (see Supplementary Video 1). (**d**) Field distribution $|E|^2$ at the transparency wavelength ($\lambda = 1067.3$ nm) in the structure with the TiO_2 layer (see Supplementary Video 2). The red arrows denote the direction of incident light. Here, $h = 250$ nm, $w = 200$ nm, $t = 20$ nm, $p = 700$ nm, $d = 1400$ nm and $g = 495$ nm.

where the fundamental mode (i.e., $m = 1$) is considered in the wavelength range of interest. By combining Eqs (1) and (2), we can achieve the theoretical wavelengths of SPP modes. As depicted in Fig. 1(b), the SPP wavelength has a red shift with increasing Al_2O_3 grating width w. There exist the symmetric and antisymmetric SPP modes in silver films[36]. The SPP mode is antisymmetric in our structures (see Supplementary Information).

To verify the theoretical results, we utilize the finite-difference time-domain (FDTD) method to simulate the optical response in the system. In the FDTD simulations, the perfectly matched layer absorbing boundary conditions are set at the top and bottom of computational space, and the periodic boundary conditions are set on the right and left sides of unit cell[37]. The real-world imperfections are not considered in the simulations, which may induce the deviation of about 5% for the spectral height between the simulations and experiments[8]. The proposed structures can be confidently realized by standard film deposition and nanofabrication equipment. As shown in Fig. 2(a,c), the structure exhibits a strong light absorption at the SPP wavelength due to the excitation of SPP mode (see Supplementary Video 1). It can be seen in Fig. 1(b) that the numerical simulations agree well with the theoretical results. To explain the shift of SPP wavelength with changing w, we plot the ERI (n_{eff}) of SPP mode as a function of w by solving Eq. (1). The inset of Fig. 1(b) shows that n_{eff} ascends with increasing w. From Eq. (2), we can see that β_{SPP} is independent on w. Thus, it is reasonable to observe the red shift of SPP wavelength with the increase of w.

Guided-mode resonance and generation of EIT-like effect. When a HRI (TiO_2) film is sandwiched in the SiO_2 layer, the guided-mode resonance can be established in the HRI layer. The dispersion relation of the TM guided mode is governed by

$$\kappa_g g = n\pi + 2 \arctan\left(\frac{\varepsilon_s}{\varepsilon_t}\frac{K_s}{\kappa_g}\right), \tag{3}$$

where $\kappa_g = (\varepsilon_t k_0^2 - \beta^2)^{1/2}$ and $K_s = (\beta^2 - \varepsilon_s k_0^2)^{1/2}$ are the wavevectors of propagation modes in the TiO_2 and SiO_2 layers, respectively. ε_t ($=n_t^2$) is the relative permittivity of TiO_2 layer. Here, the guided mode order n is set as 1. When the incident light only passes through the dielectric layers, the guided mode in HRI layer can not be excited directly (see Supplementary Information). As depicted in Fig. 2(a), a narrow transparency window occurs in the middle of the original absorption spectrum. By solving Eqs (1) and (3), the obtained dispersion curves of SPP and guided modes intersect at the transparency wavelength, as shown in the inset of Fig. 2(a). The SPP and guided modes will strongly couple with each other through the evanescent fields under the wavevector matching condition. The coupling between plasmonic and photonic modes contributes to the formation of EIT-like spectrum[38]. This is different from the coupling between localized and delocalized SPPs in graphene EIT-like systems[39]. The low-loss dielectric structure can effectively improve the Q factor of EIT-like effect[8]. To further analyze the mechanism of the EIT-like effect, we plot a prototype three-level system in Fig. 2(b). Here, the SPP mode on the metal is in analogy to the upper state $|1\rangle$. When the light (analogous to the probe field) is incident on the structure, the SPP mode will be excited on the metal (corresponds to the transition from the ground state $|0\rangle$ to $|1\rangle$). When the wavevector of SPP mode approaches that of guided mode (in analogy to the state $|2\rangle$), the strong coupling (analogous to the pump field) will be generated through the evanescent fields between the SPP and guided modes (corresponds to the transition between $|1\rangle$ and $|2\rangle$). The guided mode in HRI layer can not be directly excited, which means that the transition from $|0\rangle$ to $|2\rangle$ is forbidden. Thus, the two possible pathways: $|0\rangle \rightarrow |1\rangle$ and $|0\rangle \rightarrow |1\rangle \rightarrow |2\rangle \rightarrow |1\rangle$ will destructively interfere and generate the EIT-like effect[12,40]. As shown in Fig. 2(d), the destructive interference between the SPP and guided modes results in the disappearance of SPP field (see Supplementary Video 2), which reduces the SPP loss and gives rises to the high Q-factor EIT-like spectral response.

Analytical theory for EIT-like effect. The two-oscillator EIT model enables to quantitatively describe the EIT-like response[12]. As shown in Fig. 1, the light is incident on the metallic film with the Al_2O_3 grating and excites the SPP mode (i.e., oscillator 1). The guided mode in the TiO_2 layer (i.e., oscillator 2) is established only by coupling with oscillator 1. As depicted in Fig. 2(b), ω_0 stands for the resonance frequency of oscillator 1 (SPP frequency), δ is the resonance frequency detuning between oscillators 1 and 2, γ_1 and γ_2 are the decaying rates from the loss in oscillators 1 and 2, respectively. $\kappa e^{i\phi}$ is the coefficient of coupling between oscillators 1 and 2, and ϕ is the coupling phase retardation[40]. When $\gamma_2 \ll \gamma_1 \ll \omega_0$, $|\delta| \ll \gamma_1$ and $|\omega - \omega_0| \ll \omega_0$, the light absorptance of the entire system can be expressed as[40]

$$A = \mathrm{Im}\left\{\frac{F(\omega - \omega_0 + \delta + i\gamma_2/2)}{(\kappa e^{i\phi})^2 - (\omega - \omega_0 + i\gamma_1/2)(\omega - \omega_0 + \delta + i\gamma_2/2)}\right\}, \quad (4)$$

where A is the imaginary part of the result obtained by solving the coupled differential equations (see Methods section). A means the ratio of the power of absorption light in the system to the power of incident light. F is an amplitude coefficient. According to Eq. (4), we can fit the simulation results of absorption spectra. As shown in Fig. 3(a), the fitting curves agree well with the simulation results, which verifies the reasonability of theoretical model. From Fig. 3(b), we can see that the EIT-like spectral width becomes narrower at the same wavelength when d increases, giving rise to the higher Q-factor induced transparency. The absorption dip increases with d, and the spectral widths on both sides of the EIT window nearly keep constant. When d increases from 1300 to 1700 nm, the dip value of EIT-like spectrum changes slowly due to the relatively strong coupling between the SPP and guided modes. When d further increases, the coupling gradually becomes weak, and thus the metal-based plasmonic loss results in the shallower absorption dip, as shown in Fig. 3(b). The Q factor of EIT-like spectrum can exceed 2000 when $d > 1700$ nm. It is not superior to the Q factor in all-dielectric structures[8], but is one order of magnitude larger than that of other plasmonic systems such as plasmonic metamaterials[11] and waveguides[18–20]. If the multiple TiO_2 layers are introduced in the system, the absorption spectrum is further split, forming higher Q-factor multiple EIT windows (see Supplementary Information). By fitting the simulation results, we can obtain the theoretical values of physical parameters in the EIT model. We plot the physical parameters γ_1, γ_2, κ, δ, and ϕ as a function of d, as shown in Fig. 3(b,c). It is found that the coupling strength κ between the SPP and guided modes successively decreases with increasing d. The detuning δ is about -1.34 THz when d approaches 1700 nm, and the decay rate γ_1 is 10 THz, which is ~500 times larger than the decay rate γ_2 ($\gamma_2 = 0.02$ THz). The phase retardation ϕ ascends slowly with increasing d, as shown in Fig. 3(c). Here, γ_1 and γ_2 can be respectively regarded as the dephasing rates of the SPP and guided modes, which nearly keep constant with the change of d. κ corresponds to the Rabi frequency in the EIT system[41]. The width of the EIT-like spectrum becomes sharper with the decrease of the Rabi frequency. For the light passing through the system, the slow-light effect will be generated due to the strong dispersion in the transparency window (see Supplementary Information). The group index can be derived from the above theoretical model[11]. We find that the group index exceeds 800 in the plasmonic system with $d = 1400$ nm, which is one order of magnitude higher than that of plasmonic metamaterials[11] and waveguides[20].

Dependence of EIT-like spectrum on physical parameters. We investigate the dependence of the EIT-like spectrum on the Al_2O_3 grating width w, which controls the wavelength of SPP mode. As shown in Fig. 4(a), the EIT-like spectral profile is sensitive to w, but the position of transparency window nearly maintains unchanged. As mentioned above, the SPP wavelength exhibits a red shift with increasing w, while the wavelength of guided mode is fixed because of the phase matching condition. Thus, the spectrum becomes asymmetric and steep on the right (left) side of induced transparency when w is smaller (larger) than 200 nm owing to the deviation between the SPP and guided-mode wavelengths. Moreover, we study the influence of the TiO_2 layer thickness g on the EIT-like spectrum. As shown in Fig. 4(b), the wavelength of induced transparency possesses a red shift when g increases, which results in the asymmetric spectra. This behavior can also be explained

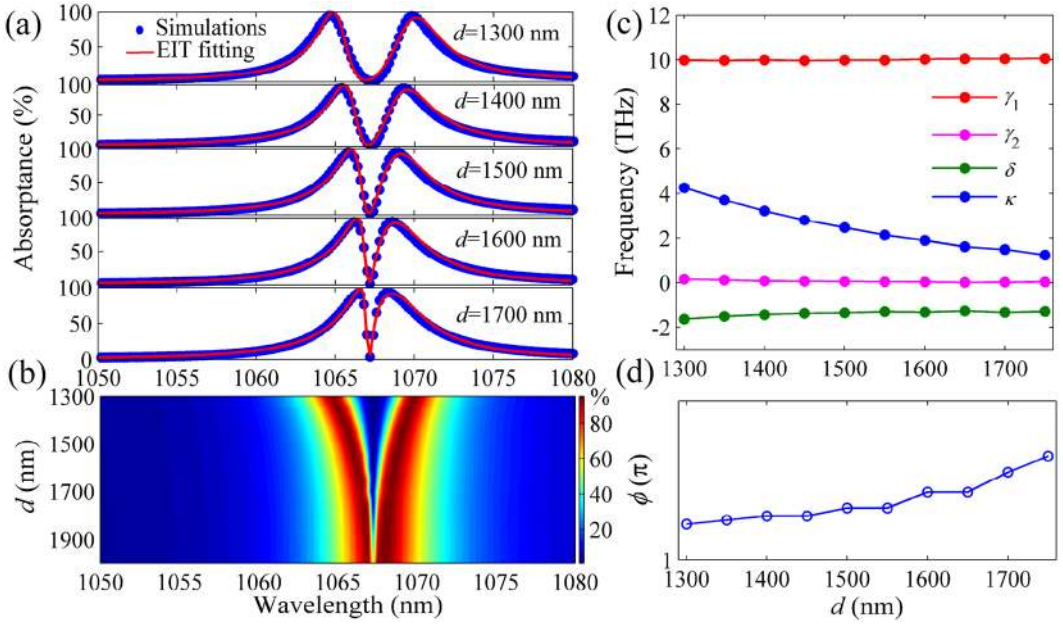

Figure 3. EIT-like response dependent on the thickness of spacer layer and fitting values of the parameters in EIT model. (**a**) Absorption spectra with different thicknesses of spacer layer *d*. The dots and curves denote the FDTD simulation and theoretical fitting results, respectively. (**b**) Evolution of absorption spectra with *d*. (**c**) Fitting values of the parameters γ_1, γ_2, κ and δ with different *d*. (**d**) Fitting results of ϕ as a function of *d*. Here, $h = 250$ nm, $w = 200$ nm, $t = 20$ nm, $p = 700$ nm and $g = 495$ nm.

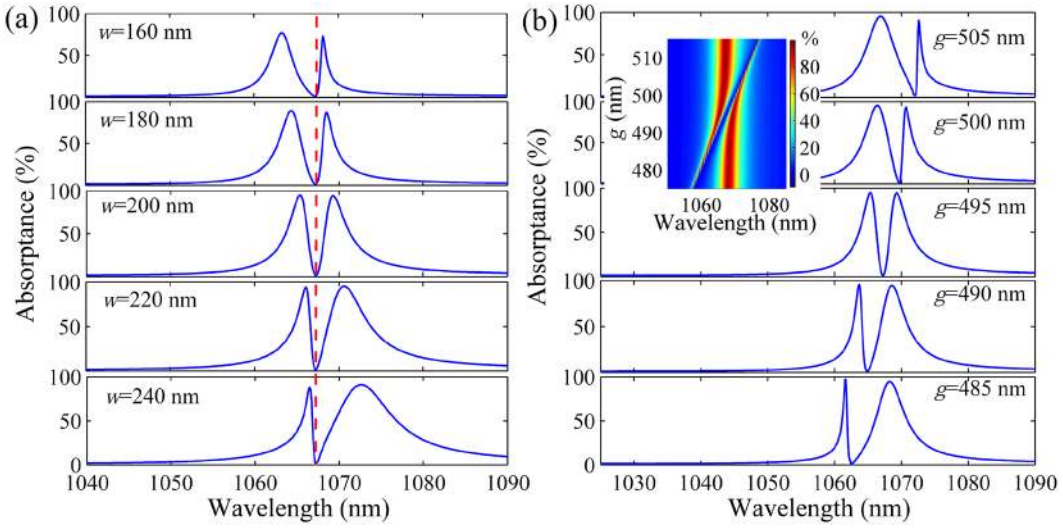

Figure 4. EIT-like response dependent on the grating width and thickness of HRI layer. Absorption spectra of the structure (**a**) with different *w* when $g = 495$ nm and (**b**) with different *g* when $w = 200$ nm. The inset shows the evolution of absorption spectrum with *g*. Here, $h = 250$ nm, $t = 20$ nm, $p = 700$ nm and $d = 1400$ nm.

by the wavevector matching condition. The ERI of the guided mode in the TiO_2 layer increases with *g* (see Supplementary Information), thus the guided-mode wavelength inevitably raises to match the wavevector of the SPP mode. The results could find applications in the spectral shaping and optical filtering. In the inset of Fig. 4(b), we can see the obvious EIT-like spectra when *g* is altered from 480 to 510 nm. It is found that the EIT wavelength has a red shift as the refractive index of HRI layer increases, as shown in Fig. 5(a). If the HRI layer is employed as a channel to pass through transparent fluidic media, the plasmonic system can work as a refractive index sensor by detecting the reflection of incident light. The figure of merit (FOM) of the sensor is about 80, which is one order of magnitude larger than that of the sensors based on the EIT-like effect in plasmonic metamaterials[27]. When a denser HRI layer (e.g. Si_3N_4) is employed, the obvious EIT-like spectrum can be achieved with selecting a larger *g* (see Supplementary Information). In addition, the EIT-like response can be obviously generated at the same

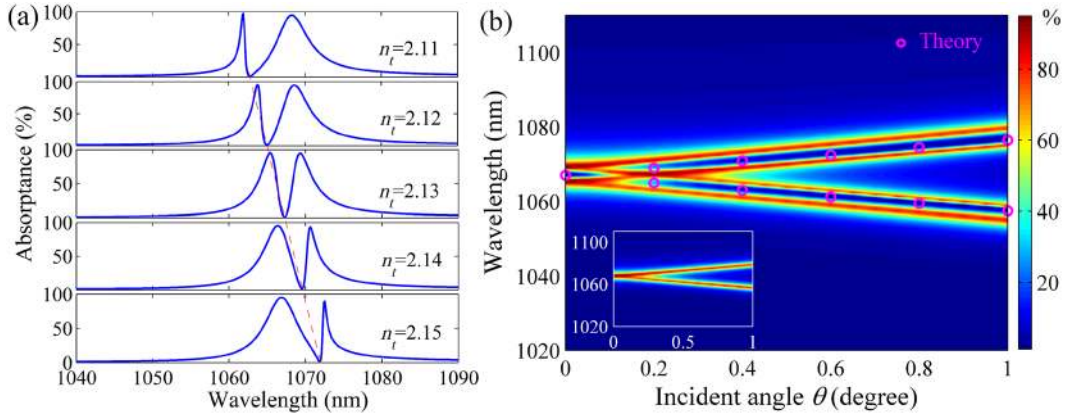

Figure 5. EIT-like response dependent on the refractive index of HRI layer and incident angle of light. (**a**) Absorption spectra of the structure with different refractive indices (n_t) of the HRI layer. (**b**) Evolution of absorption spectrum with θ in the structure with the TiO_2 layer. The circles present the theoretical wavelengths of guided mode in the TiO_2 layer. The inset shows the absorption spectrum evolution with θ in the structure without the TiO_2 layer. Here, $h = 250$ nm, $w = 200$ nm, $t = 20$ nm, $p = 700$ nm, $d = 1400$ nm and $g = 495$ nm.

wavelength when the dissipative loss of metal changes (see Supplementary Information). These features contribute to the flexible selection of HRI and metal materials in the experiments.

From Eq. (2), we can see that the SPP mode is dependent on the incident angle of light θ, which thereby enables to realize the angle-tuned EIT-like spectrum. Figure 5(b) depicts the evolution of absorption spectrum with θ. It shows that an obvious EIT pair (i.e., double EIT-like transparency windows) is formed in the splitting absorption spectrum with increasing θ. This phenomenon can be interpreted by the wavevector matching mechanism. When the light obliquely impinges on the system, two different SPP modes in the $\pm x$ axis directions will be generated on the metal, corresponding to the symbol $\pm m$ ($m = 1$) in Eq. (2). The propagation constant of the SPP mode will increase (decrease) for $+1$ (-1) order mode with increasing θ, which gives rise to the blue (red) shift for SPP wavelengths. It results in the splitting of absorption spectrum, as shown in the inset of Fig. 5(b). To remain the match between the wavevectors of the SPP and guided modes, meanwhile, the guided-mode wavelength will possess a blue (red) shift for $+1$ (-1) order SPP mode. Thus, the coupling of guided modes destructively interferes with the SPP modes, giving rise to the generation of the EIT pair. By solving Eqs (2) and (3), we can obtain the theoretical wavelengths of guided modes, which are in accordance with the positions of transparency windows of the EIT pair, as shown in Fig. 5(b). The theoretical results agree well with the FDTD simulations. These results will offer a significant guide for the geometrical design in experiments. The angle sensitivity is ~10 nm/degree, which is higher than the reports in other metallic structures[42,43]. In practice, the collimation package can be used to reduce the influence of light beam divergence on the EIT-like response.

Tunability of EIT-like response based on grapheme. Finally, we investigate the active control of the EIT-like response, which is crucial for the realization of active photonic devices. Graphene, a two-dimensional (2D) crystal of carbon atoms, attracts broad attentions because of its excellent properties containing the ultra-wide operating wavelength range and ultra-high carrier mobility[44–47]. Especially, the surface conductivity of graphene relies on the Fermi level E_f, which can be dynamically tuned via chemical doping or gate voltage[46–49]. The graphene can facilitate the active modulation of light in photonic structures[48,49]. We propose to insert a graphene monolayer in the middle of the HRI layer for the sufficient interaction between the guided mode and graphene, which is achievable in the experiments[50]. Due to the interband transition of electrons in graphene, the photons of energy $\hbar\omega > 2E_f$ for the guided mode will be absorbed by graphene, which hinders the generation of EIT-like spectrum. This mechanism is different from that of graphene plasmonic systems[51]. Here, the surface conductivity σ_g of graphene can be derived according to the random-phase approximation in the local limit (see Methods section). The carrier mobility of graphene is assumed as 10000 $cm^2V^{-1}s^{-1}$. Thus, the relative permittivity of graphene can be set as $\varepsilon_g = 2.5 + i\sigma_g/(\omega\varepsilon_0\Delta)$, where $\Delta = 0.34$ nm is the practical thickness of graphene monolayer. As shown in Fig. 6(a), the EIT-like spectrum becomes not obvious when $E_f = 0$ eV, while a narrow transparency window distinctly appears when $E_f = 0.65$ eV at the wavelength of 1067.3 nm. This is because the photon energy at this wavelength is ~1.16 eV less than $2E_f$ (=1.3 eV), and thus the incident light can not be strongly absorbed by graphene monolayer. As shown in Fig. 6(b), the imaginary part of graphene relative permittivity corresponds to the dissipative loss of graphene, which drastically decreases with increasing E_f near 0.58 eV at the wavelength of 1067.3 nm. Thus, the light absorption of the system will descend when E_f increases. By fitting the spectra with the theoretical model, we find that γ_2 decreases from 1.88 THz to 0.74 THz when E_f changes from 0 eV to 0.65 eV, while γ_1 is almost unchanged. Therefore, the EIT-like spectrum is dependent on the dephasing rate of guided mode, which can be controlled by the Fermi level of graphene. When the graphene is placed above the HRI layer, the EIT-like spectrum can also be tuned by adjusting E_f. It is difficult for the ultrathin graphene to affect the wavelength of guided mode in HRI layer, so the induced transparency position is not sensitive to the change of the Fermi level. If the HRI layer is a stack of 2D media (e.g. graphene and MoS_2)[52,53], the tunable

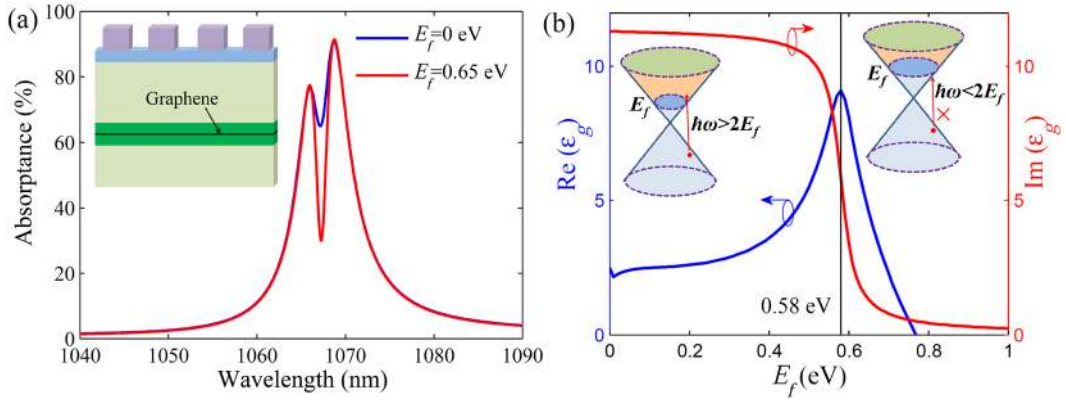

Figure 6. Graphene-controlled EIT-like response. (**a**) Absorption spectra of the graphene-assisted structure with different Fermi levels E_f for graphene. The inset shows the graphene-assisted structure. (**b**) Real and imaginary parts of the relative permittivities of graphene with different E_f at the wavelength of 1067.3 nm. The insets describe the interband transitions of graphene with different E_f. Here, $h = 250$ nm, $w = 200$ nm, $t = 20$ nm, $p = 700$ nm, $d = 1700$ nm and $g = 495$ nm.

EIT-like response can also be achieved (see Supplementary Information). The graphene-controlled EIT-like spectrum provides a promising avenue to realize active optical devices such as switches and modulators[46].

Discussion

We have presented a flexibly tunable and ultrahigh Q-factor EIT-like effect in a new plasmonic system composed of a Al_2O_3 grating and a silver film coated on the $SiO_2/TiO_2/SiO_2$ layers. The results show that the induced transparency is generated in the strong absorption spectrum when the SPP mode excited on the silver film satisfies the wavevector matching condition with the guided mode in the (TiO_2) HRI layer. The Q factor of EIT-like response can exceed 2000, which is one order of magnitude larger than that of other plasmonic systems such as plasmonic metamaterials and waveguides. The lineshape and position of EIT-like spectrum can be tailored by controlling the spacer thickness, grating width, HRI layer thickness and refractive index of HRI layer. When the light is obliquely incident, an EIT pair is generated in the splitting absorption spectrum, which can be tuned by adjusting the incident angle of light. Particularly, we introduce graphene in the HRI layer and achieve the dynamic tunability of EIT-like response by controlling the Fermi level of graphene. These results could find significant applications in high-performance plasmonic sensing, spectral shaping and switching.

Methods

To theoretically analyze the EIT-like effect, the simple two-oscillator EIT model can be utilized to quantitatively describe the spectral response[12,14,41]. In plasmonic systems, the formula of the light absorptance can be derived from the coupled differential equations, which are described as follows,

$$\begin{cases} \dfrac{\partial^2 q_1(t)}{\partial t^2} + \gamma_1 \dfrac{\partial q_1(t)}{\partial t} + \omega_0^2 q_1(t) + \kappa_c q_2(t) = \eta E_{ex}(t) \\ \dfrac{\partial^2 q_2(t)}{\partial t^2} + \gamma_2 \dfrac{\partial q_2(t)}{\partial t} + (\omega_0 - \delta)^2 q_2(t) + \kappa_c q_1(t) = 0, \end{cases} \tag{5}$$

where $q_1(t)$ and $q_2(t)$ represent the field amplitudes in oscillators 1 and 2, respectively. $E_{ex}(t)$ is the incident electric field. $\kappa_c = \kappa e^{i\phi}$ is the coupling coefficient between oscillators 1 and 2. η stands for the coupling strength between the incident light and oscillator 1.

The surface conductivity of graphene can be derived by the random-phase approximation (RPA) in the local limit[54]. The surface conductivity of single-layer graphene can be quantitatively described as

$$\begin{aligned} \sigma_g = {} & i\frac{2e^2 k_B T}{\pi\hbar^2(\omega + i\tau^{-1})} \ln\left[2\cosh\left(\frac{E_f}{2k_B T}\right)\right] \\ & + \frac{e^2}{4\hbar}\left[\frac{1}{2} + \frac{1}{\pi}\arctan\left(\frac{\hbar\omega - 2E_f}{2k_B T}\right) - \frac{i}{2\pi}\ln\frac{\left(\hbar\omega + 2E_f\right)^2}{\left(\hbar\omega - 2E_f\right)^2 + (2k_B T)^2}\right], \end{aligned} \tag{6}$$

where e is the electron charge, T is the temperature, k_B is the Boltzmann's constant, $\hbar$ is the reduced Planck's constant, ω is the angular frequency of incident light in vacuum, E_f is the Fermi level of graphene and τ stands for the charge carrier relaxation time. For graphene, τ is dependent on the carrier mobility μ and could be obtained by $\tau = \mu E_f/(ev_f^2)$. The previous reports showed that μ of graphene on the SiO_2 layer could approach 40000 $cm^2V^{-1}s^{-1}$ at room temperature[55]. In order to ensure the credibility of results, a reasonable carrier mobility of 10000 $cm^2V^{-1}s^{-1}$ is selected in the calculations. The Fermi velocity v_f is 10^6 m/s.

References

1. Harris, S. Electromagnetically induced transparency. *Phys. Today* **50**, 36 (1997).
2. Fleischhauer, M., Imamoglu, A. & Marangos, J. Electromagnetically induced transparency: optics in coherent media. *Rev. Mod. Phys.* **77**, 633–673 (2005).
3. Hau, L. V., Harris, S. E., Dutton, Z. & Behroozi, C. H. Light Speed reduction to 17 metres per second in an ultracold atomic gas. *Nature* **397**, 594–598 (1999).
4. Qi, J. *et al*. Measurement of transition dipole moments in lithium dimers using electromagnetically induced transparency. *Phys. Rev. Lett.* **88**, 173003 (2002).
5. Light, P. S., Benabid, F., Pearce, G. J., Couny, F. & Bird, D. M. Electromagnetically induced transparency in acetylene molecules with counterpropagating beams in V and Λ schemes. *Appl. Phys. Lett.* **94**, 141103 (2009).
6. Lazoudis, A. *et al*. Electromagnetically induced transparency in an open V-type molecular system. *Phys. Rev. A* **83**, 063419 (2011).
7. Naweed, A., Farca, G., Shopova, S. I. & Rosenberger, A. Induced transparency and absorption in coupled whispering-gallery microresonators. *Phys. Rev. A* **71**, 043804 (2005).
8. Xu, Q. *et al*. Experimental realization of an on-chip all-optical analogue to electromagnetically induced transparency. *Phys. Rev. Lett.* **96**, 123901 (2006).
9. Xiao, Y., Zou, X., Jiang, W., Chen, Y. & Guo, G. Analog to multiple electromagnetically induced transparency in all-optical drop-filter systems. *Phys. Rev. A* **75**, 063833 (2007).
10. Totsuka, K., Kobayashi, N. & Tomita, M. Slow light in coupled-resonator-induced transparency. *Phys. Rev. Lett.* **98**, 213904 (2007).
11. Zhang, S., Genov, D., Wang, Y., Liu, M. & Zhang, X. Plasmon-induced transparency in metamaterials. *Phys. Rev. Lett.* **101**, 047401 (2008).
12. Liu, N. *et al*. Plasmonic analogue of electromagnetically induced transparency at the Drude damping limit. *Nat. Mater.* **8**, 758–762 (2009).
13. Chiam, S. *et al*. Analogue of electromagnetically induced transparency in a terahertz metamaterial. *Phys. Rev. B* **80**, 153103 (2009).
14. Gu, J. *et al*. Active control of electromagnetically induced transparency analogue in terahertz metamaterials. *Nat. Commun.* **3**, 1151 (2012).
15. Deng, Z. L. *et al*. Full controlling of Fano resonances in metal-slit superlattice. *Sci. Rep.* **5**, 18461 (2015).
16. Deng, Z. L., Fu, T., Ouyang, Z. & Wang, G. Trimeric metasurfaces for independent control of bright and dark modes of Fano resonances. *Appl. Phys. Lett.* **108**, 081109 (2016).
17. Deng, Z., Li, X., Fu, T. & Wang, G. Fano resonance in a metasurface composed of graphene ribbon superlattice. *IEEE Photon. J.* **9**, 4801107 (2017).
18. Kekatpure, R., Barnard, E., Cai, W. & Brongersma, M. Phase-coupled plasmon-induced transparency. *Phys. Rev. Lett.* **104**, 243902 (2010).
19. Han, Z. & Bozhevolnyi, S. Plasmon-induced transparency with detuned ultracompact Fabry-Perot resonators in integrated plasmonic devices. *Opt. Express* **19**, 3251–3257 (2011).
20. Lu, H., Liu, X. & Mao, D. Plasmonic analog of electromagnetically induced transparency in multi-nanoresonator-coupled waveguide systems. *Phys. Rev. A* **85**, 053803 (2012).
21. Deng, Z. & Dong, J. Lasing in plasmon-induced transparency nanocavity. *Opt. Express* **21**, 20291–20302 (2013).
22. Ishii, S., Shalaginov, M., Babicheva, V., Boltasseva, A. & Kildishev, A. Plasmonic waveguides cladded by hyperbolic metamaterials. *Opt. Lett.* **39**, 4663–4666 (2014).
23. Lu, H., Gong, Y., Mao, D., Gan, X. & Zhao, J. L. Strong plasmonic confinement and optical force in phosphorene pairs. *Opt. Express* **25**, 5255–5263 (2017).
24. Ishii, S. *et al*. Wavelength-selective spin-current generator using infrared plasmonic metamaterials. *APL Photon.* **2**, 106103 (2017).
25. Yue, Z., Cai, B., Wang, L., Wang, X. & Gu, M. Intrinsically core-shell plasmonic dielectric nanostructures with ultrahigh refractive index. *Sci Adv.* **2**, e1501536 (2016).
26. Cai, B., Li, X., Zhang, Y. & Jia, B. Significant light absorption enhancement in silicon thin film tandem solar cells with metallic nanoparticles. *Nanotechnol.* **27**, 195401 (2016).
27. Liu, N. *et al*. Planar metamaterial analogue of electromagnetically induced transparency for plasmonic sensing. *Nano Lett.* **10**, 1103–1107 (2010).
28. Lu, H., Liu, X., Wang, G. & Mao, D. Tunable high-channel-count bandpass plasmonic filters based on an analogue of electromagnetically induced transparency. *Nanotechnol.* **23**, 444003 (2012).
29. Xu, Q., Shakya, J. & Lipson, M. Direct measurement of tunable optical delays on chip analogue to electromagnetically induced transparency. *Opt. Express* **14**, 6463–6468 (2006).
30. Chen, J., Li, Z., Yue, S., Xiao, J. & Gong, Q. Plasmon-induced transparency in asymmetric T-shape single slit. *Nano Lett.* **12**, 2494–2498 (2012).
31. Duan, X., Chen, S., Cheng, H., Li, Z. & Tian, J. Dynamically tunable plasmonically induced transparency by planar hybrid metamaterial. *Opt. Lett.* **38**, 483–485 (2013).
32. Huang, M., Zhou, Y. & Hasnain, C. A surface-emitting laser incorporating a high-index-contrast subwavelength grating. *Nat. Photon.* **1**, 119–122 (2007).
33. Zhang, T., Chen, L., Wang, B. & Li, X. Tunable broadband plasmonic field enhancement on a graphene surface using a normal-incidence plane wave at mid-infrared frequencies. *Sci. Rep.* **5**, 11195 (2015).
34. Johnson, P. & Christy, R. Optical Constants of the Noble Metals. *Phys. Rev. B* **6**, 4370 (1972).
35. Hu, F., Yi, H. & Zhou, Z. Wavelength demultiplexing structure based on arrayed plasmonic slot cavities. *Opt. Lett.* **36**, 1500–1502 (2011).
36. Andrew, P. & Barnes, W. Energy transfer across a metal film mediated by surface plasmon polaritons. *Science* **306**, 1002–1005 (2004).
37. Taflove, A. & Hagness, S. Computational Electrodynamics: The Finite-Difference Time-Domain Method (Artech House, Boston, MA 2000).
38. Tang, B., Dai, L. & Jiang, C. Electromagnetically induced transparency in hybrid plasmonic-dielectric system. *Opt. Express* **19**, 628–637 (2011).
39. Yu, R., Alaee, R., Lederer, F. & Rockstuhl, C. Manipulating the interaction between localized and delocalized surface plasmon-polaritons in graphene. *Phys. Rev. B* **90**, 085409 (2014).
40. Taubert, R., Hentschel, M., Kastel, J. & Giessen, H. Classical analog of electromagnetically induced absorption in plasmonics. *Nano Lett.* **12**, 1367–1371 (2012).
41. Garrido-Alzar, C. L., Martinez, M. A. & Nussenzveig, P. Classical analog of electromagnetically induced transparency. *Am. J. Phys.* **70**, 37 (2002).
42. Christ, A., Tikhodeev, S., Gippius, N., Kuhl, J. & Giessen, H. Waveguide-plasmon polaritons: strong coupling of photonic and electronic resonances in a metallic photonic crystal slab. *Phys. Rev. Lett.* **91**, 183901 (2003).
43. Christ, A. *et al*. Controlling the interaction between localized and delocalized surface plasmon modes: experiment and numerical calculations. *Phys. Rev. B* **74**, 155435 (2006).
44. Lu, H., Gan, X., Mao, D. & Zhao, J. Graphene-supported manipulation of surface plasmon polaritons in metallic nanowaveguides. *Photon. Res.* **5**, 162–167 (2017).

45. Sun, Z. & Chang, H. Graphene and graphene-like two-dimensional materials in photodetection: mechanisms and methodology. *ACS Nano* **8**, 4133–4156 (2014).
46. Bao, Q. & Loh, K. Graphene photonics, plasmonics, and broadband optoelectronic devices. *ACS Nano* **6**, 3677–3694 (2012).
47. Lu, H. *et al*. Graphene-based active slow surface plasmon polaritons. *Sci. Rep.* **5**, 8443 (2015).
48. Yu, R., Pruneri, V. & Abajo, F. Resonant visible light modulation with graphene. *ACS Photon.* **2**, 550–558 (2015).
49. Yu, R., Pruneri, V. & Abajo, F. Active modulation of visible light with graphene-loaded ultrathin metal plasmonic antennas. *Sci. Rep.* **6**, 32144 (2016).
50. Furchi, M. *et al*. Microcavity-integrated graphene photodetector. *Nano Lett.* **12**, 2773–2777 (2012).
51. Jiang, J. *et al*. Dynamically tunable electromagnetically induced reflection in terahertz complementary graphene metamaterials. *Opt. Mater. Express* **5**, 1962–1971 (2015).
52. Kim, K. *et al*. Synthesis and characterization of hexagonal boron nitride film as a dielectric layer for graphene devices. *ACS Nano* **6**, 8583–8590 (2012).
53. Mattheakis, M., Valagiannopoulos, C. A. & Kaxiras, E. Epsilon-near-zero behavior from plasmonic Dirac point: Theory and realization using two-dimensional materials. *Phys. Rev.* **B 94**, 201404(R) (2016).
54. Yao, Y. *et al*. Electrically tunable metasurface perfect absorbers for ultrathin mid-infrared optical modulators. *Nano Lett.* **14**, 6526–6532 (2014).
55. Chen, J., Jang, C., Xiao, S., Ishigami, M. & Fuhrer, M. Intrinsic and extrinsic performance limits of graphene devices on SiO_2. *Nat. Nanotechnol.* **3**, 206–209 (2008).

Acknowledgements

This work was supported by the National Key R&D Program of China (2017YFA0303800), National Natural Science Foundation of China (11634010, 11774290, 61705186 and 61377035), Natural Science Basic Research Plan in Shaanxi Province of China (2017JQ1023), Technology Foundation for Selected Overseas Chinese Scholar of Shaanxi Province (2017007) and Fundamental Research Funds for the Central Universities (3102016OQD031).

Author Contributions

H.L. conceived the idea, carried out the theoretical calculations and numerical simulations, as well as wrote the manuscript text. X.T.G., D.M., B.H.J. and J.L.Z. discussed the proposed plasmonic structure and analyzed the results. B.H.J. and J.L.Z. promoted the manuscript presentation. All authors substantially contributed to the manuscript.

Additional Information

Supplementary information accompanies this paper at https://doi.org/10.1038/s41598-018-19869-y.

Competing Interests: The authors declare that they have no competing interests.

Publisher's note: Springer Nature remains neutral with regard to jurisdictional claims in published maps and institutional affiliations.